the data shown in Fig. 2, it is well known that for gas breakdown induced by classical microwave fields, the threshold intensity does increase with the square of the frequency (assuming that the frequency is much greater than the electron collision frequency), and it is expected that this classical behavior will no longer be observed as the input photon energy approaches the excitation energy of the gas.

Table I gives threshold intensities at a pressure of 2000 Torr. From the Nd and ruby maser data for the five noble gases, we see that the thresholds are inversely related to ionization potential, except for He and Ne. This is not surprising if the breakdown results from a cascade growth process, since for low electron energies, the electron-atom collision cross section is higher for He than for Ne.[6]

As indicated in Table I, the input pulse durations and focused spot sizes were not identical at each wavelength. It has been observed that the threshold intensities decrease with increasing pulse duration and focal volume. The focal-volume dependence apparently arises from a diffusionlike loss mechanism.[2] Nevertheless, if the data in Fig. 2 were adjusted by redefining the threshold intensity as the average intensity over the duration of the threshold pulse, and adding an empirical correction for the focal-volume dependence, the conclusions of this Letter would remain unchanged. However, the absolute values of the threshold intensities for the 0.53 and 0.35μ radiation would be lower.

Preparatory experiments with the 0.53μ radiation revealed a cloud of bright scattering centers in the beam, which could be seen even with the focusing lens removed. This phenomenon was apparently due to impurities in the gas, and was substantially eliminated by scrupulously drying the breakdown chamber. Although the effect produced negligible attenuation of the input beam, it did tend to raise the breakdown threshold intensity, particularly at high pressures. The greater sensitivity of the eye at 0.53 μ may account for the fact that no such effect was observed at the other three wavelengths.

*The work reported in this paper was supported in part by Contract No. AF 33(615)-2287 between Air Force Avionics Laboratory, Research and Technology Division, Air Force Systems Command, U. S. Air Force, Wright-Patterson Air Force Base, Ohio, and the Ohio State University Research Foundation.

†Present address: United Aircraft Research Laboratories, East Hartford, Connecticut.

[1]R. G. Tomlinson, E. K. Damon, and H. T. Buscher, in Proceedings of the Physics of Quantum Electronics Conference (to be published).

[2]A. F. Haught, R. G. Meyerand, Jr., and D. C. Smith, in Proceedings of the Physics of Quantum Electronics Conference (to be published).

[3]S. A. Akhmanov, A. I. Kovrigin, M. M. Strukov, and R. V. Khokhlov, Zh. Eksperim. i Teor. Fiz.—Pisma Redakt. 1, 25 (1965) [translation: Soviet Phys.—JETP Letters 1, 25 (1965)].

[4]R. G. Tomlinson, Phys. Rev. Letters 14, 489 (1965).

[5]R. G. Tomlinson, J. Appl. Phys. 36, 1 (1965).

[6]E. U. Condon and H. Odishaw, Handbook of Physics, (McGraw-Hill Book Company, Inc., New York, 1958), p. 4-160

DIRECT EXPERIMENTAL TEST OF THE PY AND CHNC INTEGRAL EQUATIONS*

P. G. Mikolaj and C. J. Pings

Division of Chemistry and Chemical Engineering, California Institute of Technology, Pasadena, California

(Received 8 November 1965)

Of the many existing theories for predicting molecular distribution functions of fluids, two that have gained recent prominence are the Percus-Yevick (PY) approximation[1] and the convoluted hypernetted chain (CHNC) approximation.[2,3] The acceptance which these two approximate theories have achieved is based on the moderately good agreement between predicted thermodynamic properties and experimental values.[4] Most of the methods used to test these theories fall into two groups. In the first group are computations based on relatively simple potential functions, e.g., the hard-sphere model, in which predicted virial coefficients are compared with exact theoretical values,[5,6] or for slightly more complicated potentials, with Monte-Carlo results.[7] In the second grouping, more realistic potentials are used, e.g., the Lennard-Jones 6-12, and the results are tested by comparing predicted distribution functions or thermodynamic properties with available experimental data.[8] As far as a test of the basic PY or CHNC theory is concerned, the first grouping suffers because,

although the equations may be rigorously tested, the results do not conform to the behavior of any real fluid. In the second group, any definite conclusions regarding the applicability of these equations is clouded by uncertainties in the potential function used in the computations. The purpose of this Letter is to report a direct and unique experimental test of the basic hypotheses underlying these two approximate theories.

The PY and CHNC equations may be derived very simply by considering the Ornstein-Zernike direct correlation function (DCF),[9] which is related to the radial distribution function (RDF) by the following equation[10,11]:

$$C(\vec{r}_{12}) = G(\vec{r}_{12}) - \rho \int C(\vec{r}_{13}) G(\vec{r}_{23}) d\vec{r}_3; \quad (1)$$

where ρ is the number of density, $C(\vec{r})$ is the DCF, and $G(\vec{r}) = g(\vec{r}) - 1$ is the net RDF. The derivation of the integral equations is then initiated by introduction of fundamental assumptions regarding the relationship of $C(\vec{r})$, $G(\vec{r})$, and the intermolecular potential function, $u(\vec{r})$. These assumptions are as follows[12,13]: for PY,

$$C(\vec{r}) = [1 + G(\vec{r})]\{1 - \exp[u(\vec{r})/kT]\}; \quad (2)$$

for CHNC,

$$C(\vec{r}) = G(\vec{r}) - \ln[1 + G(\vec{r})] - u(\vec{r})/kT. \quad (3)$$

The usual form of the PY approximation is then obtained by eliminating $C(\vec{r})$ from Eqs. (1) and (2) and the CHNC approximation from a similar treatment of Eqs. (1) and (3).

If the DCF and the RDF are known, Eqs. (2) and (3) provide the most direct test regarding the applicability of these two theories. Moreover, this test is unique in that no further assumptions are required regarding the nature of the potential function. This becomes evident by solving the equations for $u(\vec{r})$:

$$[u(\vec{r})]_{\mathrm{CHNC}} = kT\{G(\vec{r}) - C(\vec{r}) - \ln[1 + G(\vec{r})]\}, \quad (4)$$

$$[u(\vec{r})]_{\mathrm{PY}} = kT \ln\left\{\frac{1 + G(\vec{r}) - C(\vec{r})}{1 + G(\vec{r})}\right\}. \quad (5)$$

If the fundamental PY and CHNC hypotheses are correct, the potential functions predicted by Eqs. (4) and (5) should obviously be independent of temperature and density, even though $G(\vec{r})$ and $C(\vec{r})$ are both state dependent. Nothing is said about the nature of the potential function that is required to satisfy these hypotheses other than the fact that it is required to be state independent.

It is apparent that, in order to perform this test, RDF and DCF data must be available over a broad range of temperature and density. We have recently computed these two functions from experimental x-ray diffraction measurements on argon at 13 states in the general vicinity of the critical region.[14,15] These measurements were made on a temperature-density grid which included isotherms (in °C) of −130, −125, −120, −110, and isochores (in g/cc) of 0.280, 0.536, 0.780, 0.910, and 0.982. (The critical temperature of argon is −122.3°C and its critical density is 0.536 g/cc.) Although the absolute temperature range is somewhat small, these measurements still provide exactly the type of information required to test the basic PY and CHNC assumptions.

The results of this test are summarized on the two accompanying figures. For conciseness we show only computations based on the PY approximation as the results for the CHNC case are essentially the same. [This is not surprising since a series expansion of the right-hand side of Eq. (5) yields lead terms identical to these of Eq. (4).] The major difference between the two approximations is that the CHNC equation predicts a potential function with a slightly broader bowl than the PY equation.

Figure 1 shows the results for the −110°C

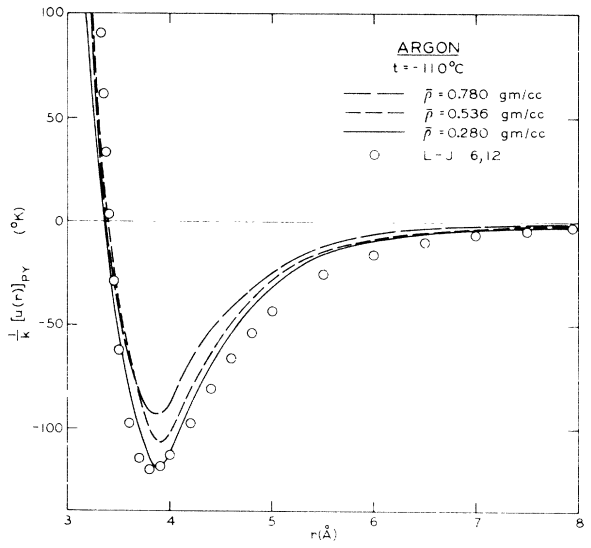

FIG. 1. Potential energy functions of argon predicted by the PY hypothesis of Eq. (5) for three densities along the −110°C isotherm. The open circles represent the 6-12 potential with parameters $\sigma = 3.405$ Å and $\epsilon/k = 119.8$°K.

isotherm. Contrary to the fundamental PY hypothesis, the predicted potential function is not independent of state. As the argon density is increased from $\rho = 0.280$ g/cc for a moderately dilute gas to that of a dense gas of $\rho = 0.780$ g/cc, the depth of the well decreases from 119 to 93°K. This same behavior is observed for the other three isotherms of our investigation. On the other hand, when a plot is made (not shown) of $[u(\vec{r})]_{PY}$ at constant density, we could discern no conclusive temperature effect within our experimental uncertainty. Also shown on Fig. 1 (as open circles), for comparison's sake, is the Lennard-Jones 6-12 potential function with parameters $\sigma = 3.405$ Å and $\epsilon/k = 119.8$°K.

This significant density effect on the predicted PY potential function, along with the negligible temperature effect over the range studied, is shown more dramatically on Fig. 2, where the depth of the well of $[u(\vec{r})]_{PY}$ is plotted against the argon density for all 13 states of our investigation. The symbols on the graph are slightly displaced from the five measured isochores in order to show our estimate of the experimental uncertainty at each state. This plot clearly shows the failure of the fundamental PY hypothesis to produce a potential function which is independent of state.

In light of these results, we conclude that the original PY and CHNC approximations are in contradiction with experimental facts for argon. In seeking to interpret these facts, we offer the following suggestions: In order to satisfy the PY and CHNC approximations, i.e., to predict a distribution function that agrees with experiment, apparently a pair potential function is required which varies with state, primarily with density. Accepting for the moment the validity of these underlying hypotheses, one may conclude that there is a significant nonadditive contribution to the true intermolecular potential. As the atomic packing becomes more congested by increasing the density, the many-body interactions become increasingly important with a net result of decreasing the effective two-body potential energy. This nonadditive contribution has been estimated to be as high as 15 to 23%, and in the same direction as we observe here.[16,17]

On the other hand, if the nonadditive forces are strictly negligible, the results of our test show that the PY and CHNC approximations require additional terms in order to produce results which are more nearly in agreement

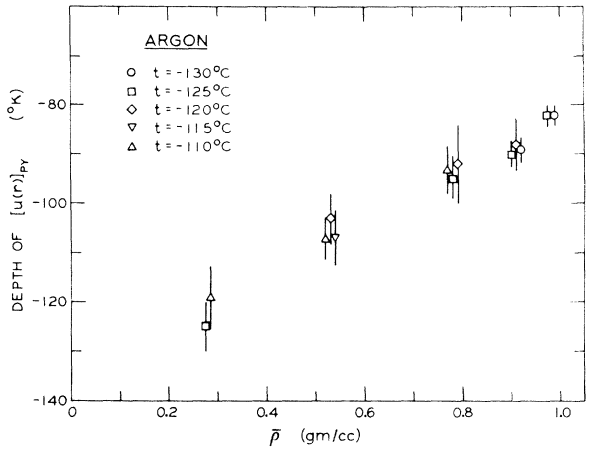

FIG. 2. Depth of the argon potential well as predicted by the PY hypothesis of Eq. (5) as a function of density at −110°C.

with experiment. This approach has been taken in the development of the so-called PY2 and CHNC2 approximations[18,19] and, most recently, by Rowlinson[13] who incorporates an empirical state-dependent factor in the original PY and CHNC hypotheses.

The authors acknowledge helpful conversations with Dr. F. P. Buff, Dr. J. L. Lebowitz, and Dr. J. C. Melrose.

*This research was supported by the Directorate of Chemical Sciences of the U. S. Air Force Office of Scientific Research, under Contract No. AF49(638)-1273, and by the Metallurgy Branch of the Office of Naval Research, under Contract No. Nonr(220)-40.

[1]J. K. Percus and G. J. Yevick, Phys. Rev. 110, 1 (1958).

[2]E. Meeron, J. Math. Phys. 1, 192 (1960).

[3]J. M. J. Van Leeuwen, J. Groeneveld, and J. De Boer, Physica 25, 792 (1959).

[4]D. Henderson, Ann. Rev. Phys. Chem. 15, 31 (1964).

[5]E. Thiele, J. Chem. Phys. 39, 474 (1963).

[6]P. Hutchinson and G. S. Rushbrooke, Physica 29, 675 (1963).

[7]A. A. Broyles, S. U. Chung, and H. L. Sahlin, J. Chem. Phys. 37, 2462 (1962).

[8]A. A. Khan, Phys. Rev. 134, A367 (1964); 136, A1260 (1964).

[9]L. S. Ornstein and F. Zernike, Proc. Acad. Sci. Amsterdam 17, 793 (1914).

[10]M. E. Fisher, J. Math. Phys. 5, 944 (1964).

[11]L. Goldstein, Phys. Rev. 84, 466 (1951).

[12]J. K. Percus, The Equilibrium Theory of Classical Fluids, edited by H. L. Frisch and J. L. Lebowitz (W. A. Benjamin, Inc., New York, 1964), p. II-33.

[13]J. S. Rowlinson, Mol. Phys. 9, 217 (1965).

[14]P. G. Mikolaj and C. J. Pings, "Radial Distribution

Functions of Argon" (to be published).
[15]P. G. Mikolaj and C. J. Pings, "Direct Correlation Functions of Argon" (to be published).
[16]L. Jansen, Phil. Mag. 8, 1305 (1963).
[17]N. R. Kestner and O. Sinanoglu, J. Chem. Phys. 38, 1730 (1963).
[18]J. K. Percus, Phys. Rev. Letters 8, 462 (1962).
[19]L. Verlet, Physica 30, 95 (1964).

DIFFERENCES IN THE CHARACTERISTIC ELECTRON ENERGY-LOSS SPECTRA OF SOLID AND LIQUID BISMUTH*

C. J. Powell

National Bureau of Standards, Washington, D. C.
(Received 1 November 1965)

A number of types of experiments have been recently performed to determine the extent to which the electronic properties of solid metals may change on melting.[1-4] The results of some experiments indicate that for certain metals the valence electron-band structure of the solid does not appear to change significantly on melting while for other metals there may be appreciable changes. Knight, Berger, and Heine[4] conclude that where there is appreciable change in the short-range atomic structure on melting, such as is known to occur for Bi and Ga, changes in the electronic properties would be expected. A report is given in this Letter of measurements of the characteristic energy loss spectra of electrons scattered by solid and liquid Bi; differences in the loss spectra are indicative of differences in the band structure of Bi in the solid and liquid states.

A Bi specimen, typically 0.5 to 1 g, was supported by a graphite rod that could be heated by electron bombardment. After melting, the specimen was approximately spheroidal in shape. A platinum versus platinum-10% rhodium thermocouple was clamped to the graphite rod about $\frac{1}{16}$ inch below the specimen and could be used to monitor the specimen temperature.

The primary electron beam, of 8-keV energy, was incident on the specimen near a vertical region at an undetermined angle. Electrons scattered through a variable known angle were decelerated to a standard energy of about 45 eV, dispersed in a hemispherical electrostatic analyzer, and detected with an electron multiplier. Characteristic loss spectra were obtained on an X-Y recorder with the multiplier output pulse rate shown as a function of the sweep voltage applied to the primary gun cathode. The measured width at half-maximum intensity of the peak of electrons scattered without energy loss was 1.6 eV.

Characteristic loss spectra of solid and liquid Bi are shown in Fig. 1 for total electron scattering angles θ of 6° and 70°. As in a previous investigation of the energy-loss spectra of evaporated Bi films,[5] peaks at ≈10 and ≈15 eV loss are observed and interpreted as being due to excitation of surface[6] and volume[7] plasmons, respectively. In the present work, however, the excitation of the surface loss predominates in both solid and liquid at $\theta = 6°$ while the volume loss predominates at $\theta = 70°$, due to the varying electron penetration.[8] It was found necessary to heat the liquid Bi initially to about 400°C to dissolve or decompose the surface oxide or other contaminating layer and so to observe the structure that changed reversibly in character across the melting point.

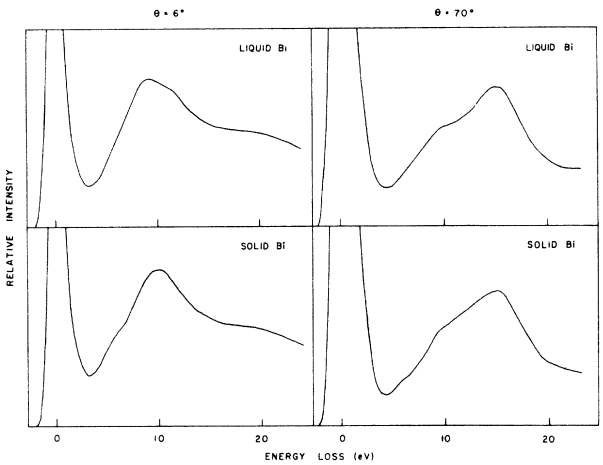

FIG. 1. Characteristic loss spectra of electrons scattered by solid and liquid Bi for total scattering angles θ of 6° and 70°.

The loss spectra of liquid and solid Bi differ in two related ways. Firstly, an additional peak is observed at 11.5 ± 0.3 eV loss in the spectrum of liquid Bi (and not in the solid), while a small loss peak is observed in the spectrum of solid